

UC Berkeley

UC Berkeley Previously Published Works

Title

Ultrahigh Bulk Photovoltaic Effect Responsivity in Thin Films: Unexpected Behavior in a Classic Ferroelectric Material

Permalink

<https://escholarship.org/uc/item/0dd8j7rb>

Journal

Solar RRL, 7(23)

ISSN

2367-198X

Authors

Shafir, Or

Bennett-Jackson, Andrew L

Will-Cole, Alexandria R

et al.

Publication Date

2023-12-01

DOI

10.1002/solr.202300294

Copyright Information

This work is made available under the terms of a Creative Commons Attribution-NonCommercial-NoDerivatives License, available at

<https://creativecommons.org/licenses/by-nc-nd/4.0/>

Peer reviewed

Ultrahigh Bulk Photovoltaic Effect Responsivity in Thin Films: Unexpected Behavior in a Classic Ferroelectric Material

Or Shafir, Andrew L. Bennett-Jackson, Alexandria R Will-Cole, Atanu Samanta, Dongfang Chen, Adrian Podpirka, Aaron Burger, Liyan Wu, Eduardo Lupi Sosa, Lane W. Martin, Jonathan E. Spanier,* and Ilya Grinberg*

The bulk photovoltaic effect (BPE) has drawn considerable attention due to its ability to generate photovoltages above the bandgap and reports of highly enhanced photovoltaic current when using nanoscale absorbers or nanoscale electrodes, which, however, do not lend themselves to practical, scalable implementation. Herein, it is shown that a strikingly high BPE photoresponse can be achieved in an ordinary thin-film configuration merely by tuning fundamental ferroelectric properties. Nonmonotonic dependence of the responsivity (R_{SC}) on the ferroelectric polarization is observed and at the optimal value of the film polarization, a more than three orders of magnitude increase in the R_{SC} from the bulk BaTiO_3 value is obtained, reaching R_{SC} close to 10^{-2} A W^{-1} , the highest value reported to date for the archetypical ferroelectric BaTiO_3 films. Results challenge the applicability of standard first-principles-based descriptions of BPE to thin films and the inherent weakness of BPE in ferroelectric thin films.

E_g , eliminating a major constraint on the PCE that leads to the Shockley–Queisser limit. Despite its promise to overcome this long-standing limit on the PCE of photovoltaic (PV) devices, BPE has been considered to be purely of academic interest for several decades following its discovery due to the high E_g of typical ferroelectrics ($>3.0 \text{ eV}$) and due to the very small photocurrents generated under illumination. The last decade has seen a resurgence of interest in the BPE with advances in its theoretical understanding and in the design of BPE materials that have led to progress toward its use in practical devices.^[7–32] First-principles-based descriptions of shift current and ballistic mechanisms of BPE showed^[15–17] that the BPE effect is impractically weak, and the generated


photocurrent is very small for both mechanisms (Table S1, Supporting Information). This is in agreement with the BPE currents observed in ceramic samples in the horizontal configuration where the sample is illuminated on the side and its top and bottom electrodes are separated by a large ($\approx 1 \text{ mm}$) distance. Several studies have showed that orders-of-magnitude higher responsivity R_{SC} (defined as the short-circuit current (J_{SC} divided by the illumination power density)) can be obtained using

1. Introduction

The bulk photovoltaic effect (BPE) in piezoelectric insulating crystals enables the generation of a photocurrent within the bulk interior of a solid and in principle, allows power conversion efficiencies (PCE) above the Shockley–Queisser limit.^[1–6] Since the excited carrier separation occurs within the bulk of the material, the open-circuit voltage of a BPE-based device can be higher than

O. Shafir, A. Samanta, I. Grinberg
Department of Chemistry
Bar-Ilan University
Ramat-Gan 5290002, Israel
E-mail: ilya.grinberg@biu.ac.il

A. L. Bennett-Jackson, A. R. Will-Cole, A. Podpirka, J. E. Spanier
Department of Materials Science & Engineering
Drexel University
Philadelphia, PA 19104-2875, USA
E-mail: spanier@drexel.edu

 The ORCID identification number(s) for the author(s) of this article can be found under <https://doi.org/10.1002/solr.202300294>.

^[†]Present address: Rice Advanced Materials Institute, Rice University, Houston, TX 77005, USA

© 2023 The Authors. Solar RRL published by Wiley-VCH GmbH. This is an open access article under the terms of the Creative Commons Attribution License, which permits use, distribution and reproduction in any medium, provided the original work is properly cited.

DOI: 10.1002/solr.202300294

D. Chen, L. Wu, J. E. Spanier
Department of Mechanical Engineering & Mechanics
Drexel University
Philadelphia, PA 19104-2875, USA

A. Burger, J. E. Spanier
Department of Electrical & Computer Engineering
Drexel University
Philadelphia, PA 19104-2875, USA

E. L. Sosa
Department of Materials Science & Engineering
University of California at Berkeley
Berkeley, CA 94720, USA

L. W. Martin^[†]
Materials Sciences Division
Lawrence Berkeley National Laboratory
Berkeley, CA 94720, USA

J. E. Spanier
Department of Physics
Drexel University
Philadelphia, PA 19104-2875, USA

nanoscale absorbers or nanoscale electrodes.^[9,13,33–35] For example, PCE above the Shockley–Queisser limit was obtained for BaTiO₃ with nanoscale electrodes.^[7] Similarly, a high R_{SC} was obtained for strained MoS₂ and WS₂ nanotubes, with an $R_{SC} \approx 1 \text{ A W}^{-1}$.^[34,35] This R_{SC} value is orders of magnitudes higher than for planar films and ceramics (Figure 1a) (We note that due to the use of different illumination intensities in experiments, R_{SC} values rather than J_{SC} values should be used when comparing the BPE photocurrents obtained in different systems). These results suggest that while standard BPE may be unsuitable for practical use, high BPE photocurrent can be obtained through special nanoscale effects present in novel 1D and 2D nanoscale systems and in thin films with precisely engineered nanoscale electrodes. However, the mechanism of these effects is currently unknown, and a path to achieving scalable BPE, that is, practical-area PV devices using such nanoscale systems or nanoscale electrodes, remains elusive.

Here, we show a more than three orders of magnitude enhancement in the BPE photocurrent responsivity in thin-film ferroelectrics compared to bulk in the classic BaTiO₃ ferroelectric, contrary to standard first-principles predictions and measurements of weak BPE. We propose that photoresponse in thin-film ferroelectrics is governed by an interplay between the generation of asymmetric distributions of excited-carrier electrons that increases with increased cation displacement and the collection of these carriers by the electrode that decreases

exponentially with increasing cation displacement.^[36] Measured responsivity R_{SC} in a simple planar-electroded ferroelectric BaTiO₃ thin film can be enhanced by more than 30-fold, to at least 10^{-2} – 10^{-1} A W^{-1} , comparable to that achieved in recent nanoscale ferroelectric systems but in a configuration that points to even higher R_{SC} and permits facile use of larger-area absorbers and electrodes and therefore practical, scalable implementation.

2. Results

2.1. Experimental Results

BaTiO₃ thin films ($\approx 50 \text{ nm}$ thick) were deposited by pulsed laser deposition on an $\approx 15 \text{ nm}$ -thick SrRuO₃ bottom-electrode layer on the following single-crystal substrates: (001)-oriented KTaO₃, (001)-oriented SrTiO₃, (110)-oriented GdScO₃, (110)-oriented DyScO₃, (110)-oriented KTaO₃, and (111)-oriented KTaO₃. The resulting heterostructures were BaTiO₃(001)/KTaO₃(001), BaTiO₃(001)/SrTiO₃(001), BaTiO₃(001)/GdScO₃(110), BaTiO₃(001)/DyScO₃(110), BaTiO₃(101)/KTaO₃(110), and BaTiO₃(111)/KTaO₃(111). For the BaTiO₃(001)/KTaO₃(001) and BaTiO₃(001)/GdScO₃(110) heterostructures, two samples were studied and are labeled as BaTiO₃(001)/KTaO₃(001) (2) and BaTiO₃(001)/GdScO₃(110) (2), respectively.

The strain and film orientation imposed by the substrate has a strong effect on the out-of-plane polarization of the grown BaTiO₃ films, allowing us to obtain a series of BaTiO₃ systems that are similar chemically but differ in the degree of polarization and structural asymmetry. Reciprocal space mapping and high-angle out-of-plane X-ray diffraction measurements were used to confirm the perovskite structure of the films and evaluate the lattice parameters of BaTiO₃. Then, we evaluated the PV response of the films under the illumination wavelengths of 365, 375, 395, and 405 nm. The obtained V_{OC} , J_{SC} , and R_{SC} are presented in Table 1 for 365 nm and in Table S2, Supporting Information for the other wavelengths. To obtain the Ti off-center displacement D , polarization P , and absorption coefficients (α) of the grown BaTiO₃ films, we use density functional theory (DFT) calculations for BaTiO₃ at the experimental lattice parameters of each film.

Examination of the experimental J – V curves (Figure 1b and S1, Supporting Information) of the (001)-oriented films shows several features characteristic of BPE, rather than the conventional junction-based effect (Section SI, Supporting Information). First, we find that the photocurrent under linearly polarized illumination shows a sinusoidal variation with the rotation of the film that is expected for BPE (Figure S2 and Section SI, Supporting Information), indicating the presence of BPE contribution. Second, experiments using BaTiO₃ doped on the *B*-site to become paraelectric at room temperature found a short-circuit current (J_{SC}) of essentially zero (Section SII, Supporting Information), strongly suggesting that the photocurrent is generated due to the presence of asymmetry in the material that gives rise to BPE.

We then analyze the J_{SC} values extracted from the J – V curves. We first normalize J_{SC} by dividing by the illumination power density to obtain the R_{SC} and plot the obtained R_{SC} values versus

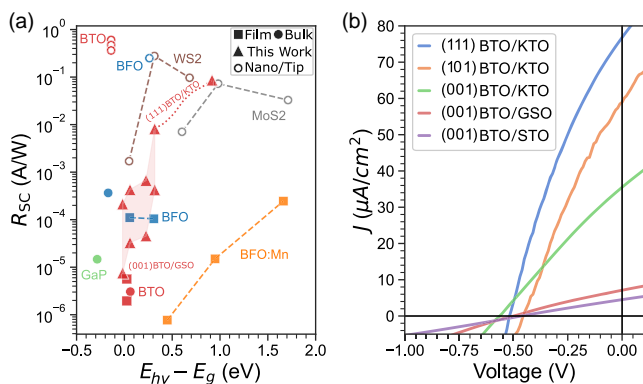


Figure 1. a) Comparison of R_{SC} as a function of incident energy above the corresponding E_g , for bulk materials (BaTiO₃ (BTO),^[6] GaP^[51,52] and BiFeO₃ (BFO)^[53]), films (BTO,^[23] BFO,^[54] and Mn-doped BFO (BFO: Mn)^[54]), nanostructures (MoS₂,^[34] WS₂ nanotubes^[33]), and tip-enhanced materials (BTO^[7] and BFO^[12]), adapted from Jiang et al.^[34] The compared values are the R_{SC} for all materials, except for bulk BTO and bulk BFO, which are the β_{31} and β_{22} BPE coefficients, respectively. The R_{SC} of all samples was measured in a vertical configuration, except for BFO:Mn and WS₂ which were studied using a lateral configuration. The R_{SC} for the BaTiO₃ films studied in this work are indicated by the shaded region with triangles marking the measurement results at the boundaries of the region. Predicted responsivity of the BaTiO₃(111)/KTaO₃(111) film at illumination 1 eV above the gap according to the variation of its absorption coefficient is shown by the red triangle connected to the shaded region by the dashed line. b) Measured photovoltaic current–voltage traces for selected 50 nm-thick BaTiO₃/KTaO₃, BaTiO₃/GdScO₃ and BaTiO₃/SrTiO₃ films under 365 nm-wavelength illumination.

Table 1. Experimental lattice parameters, DFT-calculated D , P , E_g , and α of each studied film, alongside their experimentally measured R_{SC} , V_{OC} , J_{SC} , and fill factor (FF) at 365 nm. Rigid shift of 1.1 eV^[55] is applied to E_g to account for the underestimation of DFT.

Film	c/a	a [Å]	c [Å]	E_g [eV]	D [Å]	P [Cm ⁻²]	α [10 ⁵ m ⁻¹]	R_{SC} [10 ⁻³ A W ⁻¹]	V_{OC} [V]	J_{SC} [μA cm ⁻²]	FF
BaTiO ₃ (111)/KTaO ₃ (111)	1.012	3.990	4.036	3.083	0.106	0.187	4.810	8.190	-0.519	77.247	0.293
BaTiO ₃ (101)/KTaO ₃ (110)	1.012	3.990	4.036	3.083	0.129	0.228	4.833	6.308	-0.456	59.484	0.322
BaTiO ₃ (001)/KTaO ₃ (001)	1.021	3.989	4.074	3.078	0.209	0.367	4.008	3.830	-0.567	35.732	0.271
BaTiO ₃ (001)/KTaO ₃ (001) (2)	1.032	3.989	4.116	3.071	0.237	0.413	3.449	2.050	-0.515	24.100	0.290
BaTiO ₃ (001)/GdScO ₃ (110)	1.041	3.968	4.130	3.089	0.244	0.427	3.241	0.771	-0.488	7.435	0.280
BaTiO ₃ (001)/GdScO ₃ (110) (2)	1.056	3.968	4.190	3.080	0.285	0.493	2.795	0.426	-0.493	5.020	0.290
BaTiO ₃ (001)/SrTiO ₃ (001)	1.058	3.990	4.223	3.054	0.310	0.525	2.697	0.484	-0.448	4.826	0.264
BaTiO ₃ (001)/DyScO ₃ (110)	1.060	3.945	4.182	3.102	0.277	0.485	2.773	0.651	-0.747	7.670	0.313

the photon energy in a log-scale plot (Figure 2a). It is observed that the R_{SC} data for the different BaTiO₃ films show two different regimes, with a linear rise in R_{SC} on log scale with photon energy observed for 405, 375, and 395 nm followed by a strong jump to much higher R_{SC} values at 365 nm. The decrease in BaTiO₃ R_{SC} values from 365 to 405 nm is quite strong (factor of 40–100). Since the E_g of BaTiO₃ is in the 3.1–3.3 eV range, we assign the difference in the response observed at 365 nm and the response at 375, 395, and 405 nm to the difference in the light absorption properties of BaTiO₃ between these wavelengths, with the response at 365 nm due to interband transitions and the response observed at 375, 395, and 405 nm to the excitations from impurity states corresponding to the long tail in the BaTiO₃ absorption spectrum.

Comparison of the R_{SC} data for the (001)-oriented films shows that for all wavelengths the R_{SC} decreases strongly (by a factor of more than 4) from the BaTiO₃(001)/KTaO₃(001) and BaTiO₃(001)/KTaO₃(001) (2) films to the BaTiO₃(001)/GdScO₃(110), BaTiO₃(001)/GdScO₃(110) (2), BaTiO₃(001)/

DyScO₃(110), and BaTiO₃(001)/SrTiO₃(001) films, despite their higher c/a ratio, out-of-plane P , and out-of-plane titanium displacement D (Figure 2a, Table 1 and S2, Supporting Information). Meanwhile, R_{SC} is zero for the nonpolar-doped BaTiO₃ sample (Section SII, Supporting Information). Comparison of the calculated E_g values for the different films shows only small E_g variations among the films (Table 1). Thus, unlike in the previous works that observed a similar trend of increasing R_{SC} with decreasing P ,^[24,37] for our systems, the changes in R_{SC} cannot be explained by the variation in E_g . Additionally, as discussed above, a drastic drop in R_{SC} is observed experimentally from 365 to 375 nm for all films, indicating that for all films, the E_g is between these two wavelengths, in agreement with the DFT calculations. Comparison of the calculated α shows that the small changes in the E_g due to the changes in the c/a of the different films lead to only small changes in absorption that cannot account for the observed large variation in the experimental R_{SC} values with strain, c/a , and out-of-plane P (Figure 2a, Table 1 and S2, Supporting Information). For example, while the R_{SC} of the BaTiO₃(001)/KTaO₃(001) is almost an order of magnitude larger than that of BaTiO₃(001)/GdScO₃(110) (2), the absorbance coefficient of BaTiO₃(001)/GdScO₃(110) (2) at 365 nm is $\approx 70\%$ of that of BaTiO₃(001)/KTaO₃(001). Therefore, we conclude that the variation in the R_{SC} is due to the effect of the structural variations among the films as manifested by the changes in the c/a , out-of-plane D , and P of the films. Thus, the results for the (001)-oriented films show a nonmonotonic dependence of R_{SC} on the out-of-plane P .

Comparison of the R_{SC} values to the results in the literature shows that the R_{SC} values of our (001)-oriented films are higher than those for ceramics and are consistent with the R_{SC} values previously obtained for thin films in vertical configurations (Figure 1). The observed trend of increasing R_{SC} with decreasing out-of-plane P and D suggests that even higher R_{SC} values will be observed for smaller out-of-plane P and D values, with peak values reached between $D = 0.0$ Å and 0.2 Å.

To decrease the out-of-plane P and D further and examine the R_{SC} values in the $D = 0.0$ – 0.2 Å range, we grew BaTiO₃ films on KTaO₃ (110) and (111) substrates, forming the BaTiO₃(101)/KTaO₃(110) and BaTiO₃(111)/KTaO₃(111) heterostructures. As expected, we obtained much higher J_{SC} that corresponds to R_{SC} of 10^{-2} A W⁻¹, which is close to the values obtained for

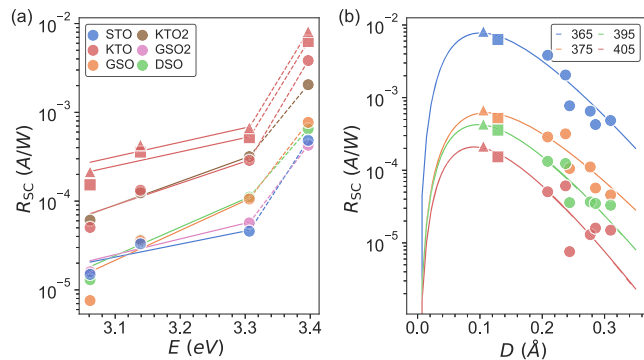


Figure 2. Different scalings of the R_{SC} for the studied samples in (001), (101), and (111) orientation marked with circle, square, and triangle, respectively. a) R_{SC} variation as a function of incident energy. Exponential fit of the R_{SC} is plotted (solid lines) for each sample and is continued by an interpolation for the higher energy (dashed lines). The films systems are abbreviated and labeled as KTO, GSO, STO, and DSO for the films grown on KTaO₃, GdScO₃, SrTiO₃, and DyScO₃ substrates, respectively. b) R_{SC} variation with D of the sample for different incident wavelengths. Plotted lines are a fitting of the values for the function of $a_0 D^3 e^{-a_1 D}$ for 365 nm and $a_0 D^2 e^{-a_1 D}$ for the other wavelengths, fitted for all of the samples.

nanoscale systems and is the largest value reported to date for BaTiO₃ films (to the best of our knowledge). The nonmonotonic dependence of R_{SC} on the out-of-plane P suggests that the magnitude of the photoresponse is controlled by more than one effect. A log-scale plot of the R_{SC} values versus the out-of-plane D (which determines the out-of-plane P) as shown in Figure 2b reveals an exponential dependence of R_{SC} on the out-of-plane D (and therefore on the out-of-plane P) in the high- D region ($D > 0.2$ Å). Therefore, for simplicity, we empirically characterize the nonmonotonic R_{SC} dependence on D as

$$R_{SC} = a_0 D^n e^{-a_1 D} \quad (1)$$

where a_0 and a_1 are constants and n is an integer. We fit the R_{SC} data to Equation (1) for $n = 1, 2$, and 3 (Figure S3, Supporting Information). We find that $n = 2$ and 3 give the best fit, with clearly poor matching between the fit and the experimental data obtained for $n = 1$. The fitting suggests that the BaTiO₃(111)/KTO₃(111) film obtains close to the maximum possible R_{SC} values at 365 nm for BaTiO₃ films. Similarly, good agreement is obtained between the R_{SC} values for illumination at 375 and 395 nm and the $D^2 e^{-a_1 D}$ scaling of R_{SC} . For 405 nm, the fit is more poor, most likely due to the large relative error (scatter) of the R_{SC} values due to the small absolute magnitude of the response to illumination at 405 nm.

Our results demonstrate, remarkably, that a larger PV response can be obtained in BaTiO₃ films by appropriately decreasing the out-of-plane polarization to $P \approx 0.18$ Cm⁻², which corresponds to an out-of-plane $D \approx 0.1$ Å. Furthermore, since BaTiO₃ has a low absorption coefficient at 365 nm, a further increase in R_{SC} can be obtained by simply using a higher photon energy of light, reaching the R_{SC} magnitudes observed for the WS₂ and MoS₂ nanoscale systems. In fact, examination of R_{SC} of different ferroelectric systems reported in the literature plotted versus the difference between the photon energy (E_{hv}) and the E_g of the ferroelectric material in Figure 1 shows that our films achieve values comparable to those of the nanoscale MoS₂ systems for the same $E_g - E_{hv}$ difference values. Thus, it is clear that even planar-electroded BaTiO₃ films can show strong photocurrent response that is much larger than that predicted by the first-principles calculations for the BPE photocurrent in BaTiO₃.^[16,17]

2.2. Interpretation and Mechanism

We now seek to identify a mechanism that would explain the empirically observed nonmonotonic dependence of R_{SC} on the out-of-plane P given by Equation (1). Since the observed $R_{SC}-P$ relationship cannot be explained either by the standard heterojunction effect, or by the model of the BPE focusing solely on the absorber, such as the first-principles approaches for calculations of the shift-current and ballistic current and the phenomenological ballistic current model, we attribute the nonmonotonic variation of R_{SC} with out-of-plane P to the combination of the effect of the asymmetry of the film leading to BPE and the effect of the Schottky barriers at the absorber–electrode interfaces.

According to the classic phenomenological theory of the ballistic BPE taking into account the FE absorber only, the short-circuit current is given by

$$J_{SC} = q l_0 \xi \phi \alpha \varphi_{opt} \quad (2)$$

where q is the electron charge, l_0 is the thermalization length, ξ is a parameter characterizing the asymmetry of the current generated by the excitation, ϕ is the quantum yield, and φ_{opt} is the photon flux. The photocurrent described by Equation (2) assumes a mechanism in which the excited electrons are sufficiently energetic to be transported over the Schottky barrier at the absorber–electrode interface.^[38] This assumption is not necessarily reasonable for the interband transitions generated by 365 nm (3.4 eV) illumination with energy that is only slightly larger than the E_g . For such illumination, the changes in the Schottky barrier height (Φ) will have a strong effect on the photocurrent collected by the electrode due to the exponential dependence of the photocurrent on the changes in the excited electron energy. For a ferroelectric–electrode interface, Φ increases with increasing out-of-plane P ,^[13,39,40] so that higher Schottky barriers and lower photocurrent can be expected for BaTiO₃ films with higher c/a , out-of-plane P , and D . On the other hand, for a non-polar material, there is no BPE so that no photocurrent is generated (In principle, a nonzero photoresponse due to the Schottky junction alone is possible. However, our experiments show an essentially zero photoresponse for the doped nonpolar BaTiO₃ film and we therefore consider the Schottky junction photoresponse to be negligible for our systems. For films where such response is significant, Equation (3) should be modified by adding a term that reflects the contribution of the Schottky junction photocurrent).

Therefore, we assign the observed decrease in the photocurrent for films with greater out-of-plane P to the higher Schottky barriers of the more strongly polar films, with the observed photocurrent described by a modification of Equation (2) as

$$J_{SC} = q l_0 \xi \phi \alpha \varphi_{opt} e^{-k\Phi} \quad (3)$$

where k is an empirical parameter and Φ is linearly proportional to the out-of-plane P (an ionic displacement) of the BaTiO₃ film.

Phenomenologically, for the ballistic current generated by the phonon mechanism, ξ is proportional to D^3 and for the impurity mechanisms it is proportional to D^2 (Section SIII and SIV, Supporting Information). Therefore, according to Equation (3), for 365 nm illumination, J_{SC} can be expected to scale as $D^n e^{-k\Phi}$ where $n = 2$ and 3 , matching the empirically fit nonmonotonic dependence of R_{SC} on out-of-plane D (Figure 2a). For excitation at below-the-gap photon energies, the asymmetry parameter ξ of the ballistic current mechanism should scale as D^2 (Section SV, Supporting Information), so that J_{SC} will scale as $D^n e^{-k\Phi}$ where $n = 1$ and 2 . Thus, R_{SC} will first increase and then decrease with increasing out-of-plane D , matching the experimentally observed trend in the R_{SC} values (Figure 2b). Using the DFT calculated values for the absorption coefficient α (Figure S4, Supporting Information) and assuming that ξ is proportional to either D^2 or D^3 we obtain excellent fits to Equation (3) for the experimentally obtained R_{SC} under illumination at 365 nm (Figure 3b) and the other illumination wavelengths (Figure S5 and S6, Supporting Information). Thus, the proposed mechanism is consistent with our R_{SC} data.

As discussed earlier, recent studies of 1D and 2D systems found high J_{SC} and R_{SC} values that were ascribed to BPE.

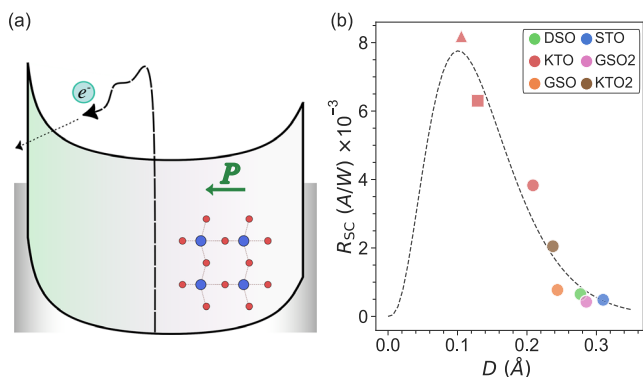


Figure 3. a) Illustration of the proposed BPE mechanism. Asymmetric momentum distribution of hot electrons in the direction of polarization is generated by BPE. The nonthermalized electrons travel ballistically toward the interface and then only a fraction of these electrons are transmitted through the Schottky barrier. b) Variation of the R_{SC} at 365 nm illumination as a function of out-of-plane D for the different samples in the (001), (101), and (111) orientations (circles, square, and triangle, respectively), together with a fit of R to $a_0 l_0 \alpha D^3 e^{-a_1 D}$ (dashed line).

Similarly, extremely high J_{SC} values and R_{SC} values were obtained for $BaTiO_3$ with nanostructured electrodes.^[7] In these studies the J - V relationship was linear. This suggests that the low gap (for the 1D and 2D systems) and the strong band bending due to nanostructured electrodes (for $BaTiO_3$)^[7] eliminate the Schottky barrier in these systems, obtaining an Ohmic contact and the corresponding high PV response. Thus, it is likely that the high performance of these system is at least in part not due to a nanoscale electrode effect per se but rather simply due to the creation of favorable Ohmic contact that allows the full collection of excited hot carriers. The consideration of the effect of the Schottky barrier can also explain the nonlinear J - V plots and the differences between these plots for the different $BaTiO_3$ systems studied in our work.

While for bulk BPE systems, a linear J - V dependence is always observed, the recently studied FE films in some cases show fairly nonlinear dependence of J on V ,^[13] while in other cases bulk-like linear or almost linear dependence of J on V has been observed.^[13,14] For our films, the $BaTiO_3(100)/GdScO_3(110)$ film has a close to linear J - V dependence, while as the out-of-plane P values decrease and the J_{SC} increases, the J - V dependence becomes more nonlinear (Figure 1b and S1, Supporting Information). However, in all cases, the V_{OC} is independent of the light intensity. We suggest that the observed variation in J - V curvature is due to the Schottky barrier effect. If the effects of Schottky barriers at the top and bottom of the film are taken into account, $J(V)$ is given by

$$J(V) = ql_0 \xi \phi \alpha \phi_{opt} e^{-\kappa_t \Phi_t} - V/d \sigma_{ph} e^{-\kappa_b \Phi_b} \quad (4)$$

where σ_{ph} is the conductivity contribution by the excited carriers, V is the applied bias, d is the thickness of the absorber (Section SV, Supporting Information), and t and b denote the top and bottom electrode, respectively. In this case, only some fraction of the excited hot carriers traveling toward the top interface (comprising J_{BPE}) and the bottom interface (comprising $J_{opposite}$) are actually

extracted into the electrode. Furthermore, the polarization of a thin film will be affected by the applied bias field and this in turn will affect the Schottky barrier height. The dependence of P on V is given by

$$P = P_0 + \epsilon V/d \quad (5)$$

where d is the thickness of the film and epsilon is the dielectric constant. Assuming a linear dependence of Φ on P , Φ is given by

$$\begin{aligned} \Phi_t &= \Phi_t^0 + \gamma_t P \\ \Phi_b &= \Phi_b^0 + \gamma_b P \end{aligned} \quad (6)$$

where γ_t and γ_b are constants. Thus, an applied bias that decreases P will lead to smaller Φ at both the top and bottom interfaces. Additionally, due to the proportionality between P and ξ , an applied bias that decreases P will, in turn, decrease ξ . It can be shown that Equation (4) predicts that more strongly nonlinear J - V curves will be obtained for films with smaller polarization, greater sensitivity of polarization to electric field, and lower thickness. In contrast, very thick films and strongly polar films will show a lower J - V curvature (Figure S7, Supporting Information). This is in agreement with the results obtained for our films. The strongly polar $BaTiO_3(100)/GdScO_3(110)$ film with high out-of-plane D , out-of-plane P , and c/a show almost linear dependence of J_{SC} on V , while the curvature of the J - V dependence increases strongly as the out-of-plane P and D decrease. We fit the J - V curves obtained for our films to Equation (4) and find that a good match with the experimental data is obtained (Figure 4a, using the fitting parameters specified in Table S3, Supporting Information). Thus, Equation (4) accurately describes the J - V curves of our $BaTiO_3$ films. Equation (4) also explains the obtained V_{OC} values which are governed by the complex interplay of intrinsic

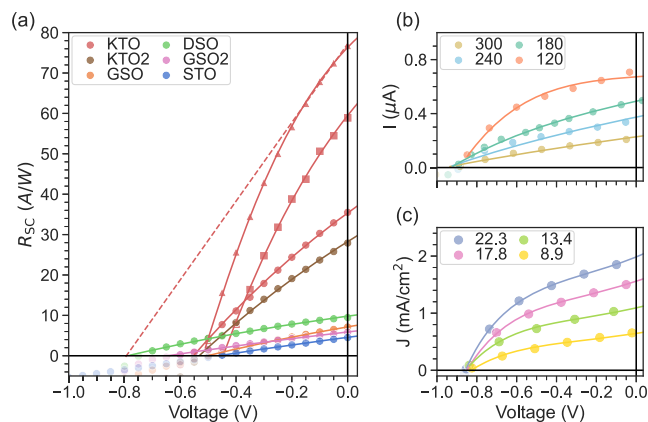


Figure 4. a) R_{SC} - V experimental data for illumination at 365 nm for our $BaTiO_3$ films (symbols) with fits of R_{SC} to the suggested model equation (solid lines), alongside an extrapolation of the initial linear response at low voltages for the $BaTiO_3(111)/KTaO_3(111)$ sample. Fitting was done for the positive R_{SC} range. b) J - V curves of films with different thicknesses (nm) studied by Tan et al.^[13] together with fits to the model suggested in this work (solid lines). c) J - V curves of PZT films under different illumination intensity ($mW\ cm^{-2}$) studied by Tan et al.^[13] together with fits to the suggested model (solid lines).

ferroelectric properties, such as P and ϵ , and the characteristics of the ferroelectric–electrode interface described by the parameters k and Φ (Section SVI, Supporting Information) (It is important to point out here that in contrast to the standard PV materials, a higher FF value is actually unfavorable for the ferroelectric systems that follow the BPE–Schottky barrier mechanism. In the absence of the Schottky barrier effect, a linear J – V relationship would be obtained, whereas due to the Schottky barrier effect, $J(V)$ decreases more rapidly (Figure S7, Supporting Information) and a lower V_{OC} is obtained. However, due to the nonlinearity of the J – V relationship, such a curve will exhibit a higher FF. Nevertheless, it is clear that the extracted power density is larger for the linear J – V relationship with a FF of 0.25 than for the nonlinearity of the J – V relationship with FF larger than 0.25 (Table S2, Supporting Information)).

An examination of the results reported in a previous study by Tan et al.^[13] suggests that they can be explained by the proposed mechanism of the joint effects of BPE and Schottky barriers expressed by Equation (4). Tan et al.^[13] studied the dependence of J_{SC} , V_{OC} , and the PCE on the film thickness in ultrathin $Pb(Zr_{0.2}Ti_{0.8})O_3$ (PZT) films. They found that J_{SC} and PCE increased with lower film thickness, reaching high values of $\approx 2 \text{ mA cm}^{-2}$ and 2.49%, respectively, for a 12 nm-thick film. Interestingly, the V_{OC} did not show a strong increase for lower film thickness and increasingly nonlinear J – V curves were observed as the film thickness changed from 300 (almost linear) to 120 nm (very curved). Tan et al.^[13] ascribed their results to the interplay between the film thickness and the Schottky barrier that creates an electric field that separates the excited charge carriers (see Section SV, Supplemental Material). However, the obtained J – V curves can be also fit well by Equation (4), as shown in Figure 4b,c (fitting parameters are presented in Table S4 and S5, Supporting Information), showing that their results are consistent with the BPE–Schottky barrier mechanism that predicts stronger J – V nonlinearity for thinner films. Several other reports of thin-film ferroelectric PV in the literature show a trend of increasing J – V nonlinearity with thinner films.^[41–43] While in several cases, these effects were ascribed to heterojunctions; in light of our results for the $BaTiO_3$ films here, it is likely that in fact they are also due to the BPE–Schottky barrier mechanism.

2.3. Possible Origin of the Strong BPE in Planar Films

We now discuss the origin of the high-BPE R_{SC} that is much higher (even in the presence of the Schottky barrier effect) than the values predicted by first-principles calculations. In a bulk ferroelectric material, ballistic photocurrent arises either from the scattering of the hot carriers from asymmetric impurities or from phonons, both of which generate an asymmetric potential that affects the Bloch states of the system. As shown by first-principles calculations,^[17] both of these effects are weak.

However, in a thin ferroelectric film, an additional source of asymmetric scattering is present that has not been considered in first-principles calculations, namely, the deviation of the film structure from periodicity near the ferroelectric–electrode interface. While ferroelectric–electrode systems are often idealized as a simple combination of ferroelectric and electrode, in practice,

the presence of the electrode affects the structure of the ferroelectric film in the vicinity of the interface, generating deviation from the bulk structure. For example, band bending and a curved electrostatic potential in the vicinity of the interface (Figure S8, Supporting Information) will lead to an aperiodic asymmetric structure close to the electrode, in contrast to the periodic asymmetric structure obtained in the presence of a linearly changing V arising from the presence of the depolarizing field. Such deviation from periodicity will act as an impurity and give rise to a ballistic photocurrent for the electrons excited in the vicinity of the ferroelectric–electrode interface. In contrast to the impurities such as defects that typically have a very low concentration, the deviation from the bulk periodic structure occurs in every unit cell of the top layers of the ferroelectric films. Thus, the asymmetric scattering that gives rise to ballistic photocurrent should be much stronger in the thin film in the vicinity of the electrode than that arising from the presence of impurities in the bulk system. We suggest that this impurity-like scattering is the origin of the extremely high R_{SC} values observed in our films and in other recent experiments on ferroelectric BPE devices. This hypothesis suggests that engineering of greater deviation from periodicity either through the modification of the ferroelectric–electrode interface or by targeted growth of impurity layers can be used to further increase the R_{SC} and PCE of ferroelectric PV devices.

3. Conclusion

Our results show that the electrode–absorber interface, the orientation of the out-of-plane P relative to the crystal axis, and the local structure can be used to enhance the photocurrent of BPE-based devices so that simple changes of the film orientation and strain conditions result in up to a factor of 20 difference in the R_{SC} and the generated photocurrent. Significantly, at the optimal value of the film polarization, a more than three orders of magnitude increase in the R_{SC} from the bulk $BaTiO_3$ value is obtained. Specifically, for the $BaTiO_3(111)/KTaO_3(111)$ film, R_{SC} reaches $\approx 10^{-2} \text{ A W}^{-1}$ in a planar-electroded device due to the weaker Φ effect that allows collection of a greater fraction of the generated bulk photocurrent. Considering the weak absorption of $BaTiO_3$ at 365 nm, R_{SC} can be increased to 10^{-1} simply by enhancing absorption using higher photon energies. Such high values of R_{SC} are comparable to those obtained for devices based on ferroelectric WS_2 and MoS_2 nanotubes and for devices based on the tip enhancement effect (Figure 1).

This suggests that the high responsivities observed in these nanoengineered systems may not be due to a nanoscale electrode effect per se or to the changes to the bulk carrier separation mechanism, but rather to the reduction of the Schottky barrier. The good fit of the experimental data obtained for our $BaTiO_3$ films to Equation (4) suggests that even for the $BaTiO_3(111)/KTaO_3(111)$ film, a Schottky barrier still exists and prevents some fraction of excited carriers from being collected by the electrodes. This suggests that a realization of an Ohmic contact should enable an even higher R_{SC} , perhaps reaching as high as 1 A W^{-1} . Thus, our results demonstrate that BPE is in fact a strong effect for thin-film systems that is often masked by the weak light absorption due to the large gap of the absorber and

by the poor carrier collection due to the Schottky barrier at the absorber–electrode interface.

With regard to applications, consideration of our results suggests the following research directions for achieving high R_{SC} and PCE in ferroelectric PV thin-film devices. First, it is vital to increase the amount of the light absorbed by the film. Second, it is necessary to eliminate the deleterious effect of the Schottky barrier to obtain a high J_{SC} , which will also tend to increase V_{OC} and PCE. Finally, to obtain a high V_{OC} , the P of the film should be stable in the presence of the applied V , allowing the favorable linear J – V relationship to be obtained. Furthermore, our results suggest that a film with a polarization gradient through the entire film thickness may exhibit a high PCE. In such a film, deviation from periodicity is obtained throughout the film rather than only in the vicinity of the FE-electrode interface, so that the ultrahigh-BPE hot-carrier scattering effect will enable photocurrent generation even in the region far from the film–electrode interface, allowing the use of thick films, which can achieve higher-than-bandgap V_{OC} simply by increasing the film thickness due to the linear dependence of V_{OC} on d . Additionally, even with a V_{OC} under the E_g , PV devices based on BPE can be used for wavelength-sensitive photodetection^[44] and for low-intensity light harvesting, due to the lack of dependence of PCE on light intensity. In theoretical research, further efforts are necessary to develop a microscopic, first-principles-based description of the strong BPE effect in thin films that incorporates the effect of the interface and enables first-principles calculations to provide guidance for further BPE device design efforts.

4. Experimental Section

The studied BaTiO₃ thin films were deposited by pulsed laser deposition (MTI and CrysTech GmbH) from solid-state SrRuO₃ and BaTiO₃ ceramic targets using a 248 nm wavelength KrF excimer laser under fluences ranging from 1.3 to 1.75 mJ cm⁻², background O₂ (g) pressures ranging from 20–75 mTorr, and a substrate temperature controller setting of 700 °C. The substrates were maintained at a distance of 6.0 cm away from the target. Reciprocal space mapping and high-angle out-of-plane X-ray diffraction measurements were performed on film heterostructures using Panalytical Empyrean 3 Rigaku SmartLab, Bruker Discovery D8 or Panalytical X'Pert³ MRD X-ray diffractometers. Shown in Figure S9, Supporting Information, are results for the (001)-oriented heterostructured BaTiO₃/SrRuO₃ films on SrTiO₃(001), DyScO₃(101), GdScO₃(101), KTaO₃(001), KTaO₃(101), and KTaO₃(111) substrates. The reciprocal space mapping studies about the $\bar{1}03$, (222), and (321) diffraction conditions of BaTiO₃ and pseudocubic orthorhombic SrRuO₃ layers confirmed that the deposited films were coherently strained with the GdScO₃, DyScO₃ and KTaO₃ substrates and compressively strained, not unexpectedly, whereas that for the SrTiO₃ showed a purely horizontal shift and broadening compared with the bulk value,^[45] consistent with (partial) strain relaxation and mosaicity of the film (Figure S9, Supporting Information). The c/a of each film was calculated from the reciprocal space mapping through a modified Bragg equation for a tetragonal unit cell (Table 1 and Section SI, Supporting Information). SrRuO₃ films and BaTiO₃/SrRuO₃ heterostructures were measured by topographic height scanning probe microscopy and determined to have root mean squared values of 0.83 nm and between 1.01 and 1.38 nm for the SrRuO₃ and BaTiO₃/SrRuO₃ heterostructures, respectively. Four-point probe resistivity measurements of the as-deposited \approx 15 nm-thick SrRuO₃ films yielded values \leq 1.7 m Ω cm. The films were single domain as shown by piezoelectric force microscopy measurements. Film

heterostructures were photolithographically patterned with square DC-sputtered (Denton Explorer 14) indium tin oxide (90 wt% In₂O₃, 10 wt % SnO₂) transparent top electrodes with a side length of 90 μ m. The PV response of the films was studied under selected illumination wavelengths of 365, 375, 395, and 405 nm. The obtained V_{OC} , J_{SC} , and R_{SC} are presented in Table 1 for 365 nm and in Table S2, Supporting Information for the other wavelengths. Data were collected under atmosphere and at room temperature using a Keithley semiconductor parameter analyzer (SCS-4200) in a Lakeshore model TTP4 probe station using narrow-spectral-linewidth LED illuminations at 365, 375, 395, and 405 nm (Thorlabs models M365LP1, M375L4, M395L4 and M405LP1, respectively) under irradiances ranging from \approx 1 to 30 mW cm⁻² using neutral density filters. Photovoltaic current data were collected on 5–7 electrode test structures for each heterostructure thin film/substrate combination using voltage sweeps from 0.1 to –1.0 V.

We used DFT calculations to obtain the D , P , and absorption coefficients (α) of BaTiO₃ at the lattice parameters of the experimental films. The D , P , and α under different c/a ratios calculations were carried out using five-atom BaTiO₃ unit cells. In each case, we imposed the experimental lattice parameters of the studied film and performed the relaxation of the internal coordinates. All of the relaxations, Schottky barrier, and bulk properties calculations were performed using the Quantum ESPRESSO package^[46] with the Perdew–Burke–Ernzerhof functional.^[47] The optical properties were calculated using the ABINIT package.^[48] In all calculations, norm-conserving pseudopotentials from the Pseudo-Dojo database were used.^[49] The calculated D , P , E_g , and α at 365 nm are presented in Table 1. The α at the other wavelengths can be found and Table S2, Supporting Information, alongside the absorption coefficient plot in Figure S4, Supporting Information. For the parameters optimization and curve fitting, basin-hopping optimization was used as implemented in the SciPy package.^[50]

Supporting Information

Supporting Information is available from the Wiley Online Library or from the author.

Acknowledgements

O.S., A.L.B.-J., and A.R.W.-C. contributed equally to this work. The authors thank V. Fridkin, R. Agarwal, and M.W. Cole for discussions. This work was supported at Bar-Ilan University and Drexel University by the NSF-BSF under grant no. CBET 1705440. The authors also acknowledge support at Bar-Ilan, Drexel, and the University of California at Berkeley from the ARO under grant no. W911NF-21-1-0126, from the NSF at Drexel under grant no. DMR 1608887, and UC Berkeley under grant no. DMR 2102895. A.L.B.-J. acknowledges support from the National Workforce Diversity Pipeline program of the Dept. of HHS under grant no. CPIMP151091. L.W.M. and J.E.S. acknowledge support from the Army/ARL under Collaborative for Hierarchical Agile and Responsive Materials (CHARM) under cooperative agreement W911NF-19-2-0119 and from the Director's Innovation Initiative under 21-C-0090. The authors also acknowledge the Singh Center for Nanotechnology by the NSF Nanotechnology Coordinated Infrastructure Program under grant no. NNCI-1542153, the Drexel University Materials Characterization Facility (NSF DMR 1040166), and K. Chen, X. Xi, and the Temple University College of Science and Technology Research Facilities.

Conflict of Interest

The authors declare no conflict of interest.

Data Availability Statement

The data that support the findings of this study are available from the corresponding author upon reasonable request.

Keywords

bulk photovoltaic effects, ferroelectrics, thin films

Received: April 23, 2023

Revised: August 1, 2023

Published online: October 18, 2023

- [1] A. Grekov, M. Ma, V. Spitsyna, V. Fridkin, *Sov. Phys. Crystallogr.* **1956**, 37, 423.
- [2] A. Glass, D. von der Linde, T. Negran, *Appl. Phys. Lett.* **1974**, 25, 233.
- [3] W. Koch, R. Munser, W. Ruppel, P. Würfel, *Solid State Commun.* **1975**, 17, 847.
- [4] V. Belinicher, B. I. Sturman, *Sov. Phys. Usp.* **1980**, 23, 199.
- [5] V. M. Fridkin, in *Photoferroelectrics*, Vol. 9, Springer, Berlin, Heidelberg **2012**, <https://doi.org/10.1007/978-3-642-81351-1>.
- [6] B. I. Sturman, V. M. Fridkin, in *Photovoltaic and Photo-Refractive Effects in Noncentrosymmetric Materials*, Routledge, London **2021**, <https://doi.org/10.1201/9780203743416>.
- [7] J. E. Spanier, V. M. Fridkin, A. M. Rappe, A. R. Akbashev, A. Polemi, Y. Qi, Z. Gu, S. M. Young, C. J. Hawley, D. Imbrenda, G. Xiao, A. L. Bennett-Jackson, C. L. Johnson, *Nat. Photonics* **2016**, 10, 611.
- [8] A. P. Kirk, D. W. Cardwell, *Nat. Photonics* **2017**, 11, 329.
- [9] J. E. Spanier, V. M. Fridkin, A. M. Rappe, A. R. Akbashev, A. Polemi, Y. Qi, Z. Gu, S. M. Young, C. J. Hawley, D. Imbrenda, G. Xiao, A. L. Bennett-Jackson, C. L. Johnson, *Nat. Photonics* **2017**, 11, 330.
- [10] R. Nechache, C. Harnagea, S. Li, L. Cardenas, W. Huang, J. Chakraborty, F. Rosei, *Nat. Photonics* **2015**, 9, 61.
- [11] R. Nechache, C. Harnagea, S. Licocchia, E. Traversa, A. Ruediger, A. Pignolet, F. Rosei, *Appl. Phys. Lett.* **2011**, 98, 202902.
- [12] M. Alexe, D. Hesse, *Nat. Commun.* **2011**, 2, 256.
- [13] Z. Tan, L. Hong, Z. Fan, J. Tian, L. Zhang, Y. Jiang, Z. Hou, D. Chen, M. Qin, M. Zeng, J. Gao, X. Lu, G. Zhou, X. Gao, J.-M. Liu, *NPG Asia Mater.* **2019**, 11, 20.
- [14] D. Cao, C. Wang, F. Zheng, W. Dong, L. Fang, M. Shen, *Nano Lett.* **2012**, 12, 2803.
- [15] S. M. Young, F. Zheng, A. M. Rappe, *Phys. Rev. Lett.* **2012**, 109, 236601.
- [16] S. M. Young, A. M. Rappe, *Phys. Rev. Lett.* **2012**, 109, 116601.
- [17] Z. Dai, A. M. Schankler, L. Gao, L. Z. Tan, A. M. Rappe, *Phys. Rev. Lett.* **2021**, 126, 177403.
- [18] Z. Dai, A. M. Rappe, *Phys. Rev. B* **2021**, 104, 235203.
- [19] G. Dalba, Y. Soldo, F. Rocca, V. Fridkin, P. Sainctavit, *Phys. Rev. Lett.* **1995**, 74, 988.
- [20] Z. Chen, M. Segev, D. W. Wilson, R. E. Muller, P. D. Maker, *Phys. Rev. Lett.* **1997**, 78, 2948.
- [21] W. Ji, K. Yao, Y. C. Liang, *Adv. Mater.* **2010**, 22, 1763.
- [22] C. Somma, K. Reimann, C. Flytzanis, T. Elsaesser, M. Woerner, *Phys. Rev. Lett.* **2014**, 112, 146602.
- [23] A. Zenkevich, Y. Matveyev, K. Maksimova, R. Gaynutdinov, A. Tolstikhina, V. Fridkin, *Phys. Rev. B* **2014**, 90, 161409.
- [24] L. You, F. Zheng, L. Fang, Y. Zhou, L. Z. Tan, Z. Zhang, G. Ma, D. Schmidt, A. Rusydi, L. Wang, L. Chang, A. M. Rappe, J. Wang, *Sci. Adv.* **2018**, 4, eaat3438.
- [25] R. Fei, L. Z. Tan, A. M. Rappe, *Phys. Rev. B* **2020**, 101, 045104.
- [26] M. Nakamura, S. Horiuchi, F. Kagawa, N. Ogawa, T. Kurumaji, Y. Tokura, M. Kawasaki, *Nat. Commun.* **2017**, 8, 281.
- [27] M. Nakamura, H. Hatada, Y. Kaneko, N. Ogawa, Y. Tokura, M. Kawasaki, *Appl. Phys. Lett.* **2018**, 113, 232901.
- [28] A. M. Burger, R. Agarwal, A. Aprelev, E. Schrubba, A. Gutierrez-Perez, V. M. Fridkin, J. E. Spanier, *Sci. Adv.* **2019**, 5, eaau5588.
- [29] A. M. Burger, L. Gao, R. Agarwal, A. Aprelev, J. E. Spanier, A. M. Rappe, V. M. Fridkin, *Phys. Rev. B* **2020**, 102, 081113.
- [30] M.-M. Yang, D. J. Kim, M. Alexe, *Science* **2018**, 360, 904.
- [31] S. Nadupalli, J. Kreisel, T. Granzow, *Sci. Adv.* **2019**, 5, 3.
- [32] Z. Gu, D. Imbrenda, A. L. Bennett-Jackson, M. Falmbigl, A. Podpirka, T. C. Parker, D. Shreiber, M. P. Ivill, V. M. Fridkin, J. E. Spanier, *Phys. Rev. Lett.* **2017**, 118, 096601.
- [33] Y. Zhang, T. Ideue, M. Onga, F. Qin, R. Suzuki, A. Zak, R. Tenne, J. Smet, Y. Iwasa, *Nature* **2019**, 570, 349.
- [34] J. Jiang, Z. Chen, Y. Hu, Y. Xiang, L. Zhang, Y. Wang, G.-C. Wang, J. Shi, *Nat. Nanotechnol.* **2021**, 16, 894.
- [35] M. Zhong, C. Yuan, X. Liu, B. Zhu, L. Meng, C. Zhou, F. Liu, J. Xu, J. Wang, G. Rao, *Mater. Lett.* **2021**, 287, 129299.
- [36] A. H. Hubmann, S. Li, S. Zhukov, H. Von Seggern, A. Klein, *J. Phys. D: Appl. Phys.* **2016**, 49, 295304.
- [37] F. Wang, S. M. Young, F. Zheng, I. Grinberg, A. M. Rappe, *Nat. Commun.* **2016**, 7, 10419.
- [38] P. Lopez-Varo, L. Bertoluzzi, J. Bisquert, M. Alexe, M. Coll, J. Huang, J. Jimenez-Tejada, T. Kirchartz, R. Nechache, F. Rosei, Y. Yuan, *Phys. Rep.* **2016**, 653, 1.
- [39] M. Stengel, P. Aguado-Puente, N. A. Spaldin, J. Junquera, *Phys. Rev. B* **2011**, 83, 235112.
- [40] F. Chen, A. Klein, *Phys. Rev. B* **2012**, 86, 094105.
- [41] N. Ramakrishnegowda, D. S. Knoche, L. Mühlenbein, A. Lotnyk, A. Bhatnagar, *ACS Appl. Nano Mater.* **2020**, 3, 11881.
- [42] G. Chen, K. Zou, Y. Yu, Y. Zhang, Q. Zhang, Y. Lu, Y. He, *Ceram. Int.* **2020**, 46, 4148.
- [43] H. Han, D. Kim, S. Chae, J. Park, S. Y. Nam, M. Choi, K. Yong, H. J. Kim, J. Son, H. M. Jang, *Nanoscale* **2018**, 10, 13261.
- [44] V. A. Balanov, F. Temerov, V. Pankratov, W. Cao, Y. Bai, *Sol. RRL* **2023**, 7, 2200995.
- [45] M. Wittels, F. Sherrill, *J. Appl. Phys.* **1957**, 28, 606.
- [46] P. Giannozzi, S. Baroni, N. Bonini, M. , R. Car, C. Cavazzoni, D. Ceresoli, G. L. Chiarotti, M. Cococcioni, I. Dabo, A. D. Corso, S. de Gironcoli, S. Fabris, G. Fratesi, R. Gebauer, U. Gerstmann, C. Gougoussis, A. Kokalj, M. Lazzeri, L. Martin-Samos, N. Marzari, F. Mauri, R. Mazzarello, S. Paolini, A. Pasquarello, L. Paulatto, C. Sbraccia, S. Scandolo, G. Scauzero, A. P. Seitsonen, A. Smogunov, et al., *J. Phys.: Condens. Matter* **2009**, 21, 395502.
- [47] J. P. Perdew, K. Burke, M. Ernzerhof, *Phys. Rev. Lett.* **1996**, 77, 3865.
- [48] X. Gonze, B. Amadon, G. Antonius, F. Arnardi, L. Baguet, J.-M. Beuken, J. Bieder, F. Bottin, J. Bouchet, E. Bousquet, N. Brouwer, F. Bruneval, G. Brunin, T. Cavignac, J.-B. Charraud, W. Chen, M. Côté, S. Cottenier, J. Denier, G. Geneste, P. Ghosez, M. Giantomassi, Y. Gillet, O. Gingras, D. R. Hamann, G. Hautier, X. He, N. Helbig, N. Holzwarth, Y. Jia, et al., *Comput. Phys. Commun.* **2020**, 248, 107042.
- [49] M. van Setten, M. Giantomassi, E. Bousquet, M. Verstraete, D. Hamann, X. Gonze, G.-M. Rignanese, *Comput. Phys. Commun.* **2018**, 226, 39.
- [50] P. Virtanen, R. Gommers, T. E. Oliphant, M. Haberland, T. Reddy, D. Cournapeau, E. Burovski, P. Peterson, W. Weckesser, J. Bright, S. J. van der Walt, M. Brett, J. Wilson, K. J. Millman, N. Mayorov, A. R. J. Nelson, E. Jones, R. Kern, E. Larson, C. J. Carey, I. Polat, Y. Feng, E. W. Moore, J. VanderPlas, D. Laxalde, J. Perktold,

- R. Cimrman, I. Henriksen, E. A. Quintero, C. R. Harris, et al., *Nat. Methods* **2020**, *17*, 261.
- [51] S. Astafiev, V. Fridkin, V. Lazarev, *Ferroelectrics* **1988**, *80*, 251.
- [52] C. Kittel, P. McEuen, P. McEuen, in *Introduction to Solid State Physics*, Vol. *8*, Wiley, New York **1996**.
- [53] T. Choi, S. Lee, Y. J. Choi, V. Kiryukhin, S. W. Cheong, *Science* **2009**, *324*, 63.
- [54] H. Matsuo, Y. Noguchi, M. Miyayama, *Nat. Commun.* **2017**, *8*, 207.
- [55] O. Shafir, J. Yang, A. M. Rappe, I. Grinberg, *J. Appl. Phys.* **2019**, *126*, 174101.